Impact of Parameters' Temporal Resolution on Surface Latent Heat Flux in the Tropical Eastern Pacific: ERA-Interim Monthly and 6-Hourly

Zachary M. Menzo[1,*]

[1] Department of Atmospheric Sciences, University of Hawai'i at Mānoa, Honolulu, HI, USA
[*] Correspondence: zmenzo@hawaii.edu

Abstract The present report tests two versions of the ECMWF Reanalysis Interim (ERAi) dataset with different temporal resolutions. Variable output from the ERAi monthly and 6-hourly versions allows for a comparison of the two datasets over a three month period. The exercise intends to determine if, when averaged over a month, will the different ERAi datasets produce similar results. NCAR's Model for Prediction Across Scales global atmospheric component (MPAS-A) uses the two ERAi versions to run simulations between December 1997 and February in the following year. Higher-resolution mesh (15km) is centered in the tropical Eastern Pacific, emphasizing regional precipitation rate and the associated variables; sea surface temperature (SST), surface latent flux (LHF), and a new convergence over evaporation (C/E) metric. SST and the C/E index shows a high degree of agreeance. However, the LHF exhibits substantial variation between the ERAi data, upwards of $\pm 50 Wm^{-2}$. Differences of this magnitude suggest against the substitution of different temporal resolutions in future investigations.

Plain Language Summary

Datasets used for scientific experiments receive updates from real-world measurements at different time intervals. Between these updates, missing values are calculated from the surrounding data (think of a line connecting two points). Two datasets are the focus of the following paper. One is updated each month and the other every six hours. However, what would happen to the data if both are average over a month? Would the data then look similar, or would there be considerable disagreement? This paper finds answers to both questions by looking at three variables between December and February in 1997-1998. Some of the variables are very similar, while others a substantially different. Therefore, it is scientifically inaccurate to substitute the 6-hourly and monthly datasets in future experiments.

Keywords: Sea surface temperature, latent heat flux, precipitation rate, tropical eastern pacific, temporal resolution, convergence, evaporation

---

1. Introduction

A persistent challenge of observing the atmosphere-ocean interface is the finite scale at which climate critical fluxes connect the two media. Subtle differences in the variables used to parameterize the fluxes may impact the exchange of momentum, heat, and moisture (Bretherton, 2018), ultimately influencing any prospective analysis. The present report aims to test one such variation by averaging datasets of different temporal resolutions over a month and quantify any resulting variation. NCAR's Model for Prediction Across Scales atmospheric component (MPAS-A) uses monthly and 6-hourly ECMWF Reanalysis Interim (ERAi) data to run simulation over a three month period. Comparison of model output is possible through the use of sea surface temperature (SST), the bulk latent heat flux (LHF) equation (Section 2.3.1.), in addition to a convergence over evaporation (C/E) index recently proposed by Torri et al. (2017) (Section 2.3.2.). After processes the datasets (Section 3), results are presented and analyzed as monthly averages for December, January, and February during the 1997-1998 El Niño event. This examination then measures any variance between the monthly and 6-hourly counterparts present in the three metrics. If found to be negligible, then either dataset may be confidently used without influencing the results of pending investigations (Section 4).

2. Background

In 2017, Torri et al. devised a way to utilize the natural fractionation of hydrogen in our atmosphere to infer information about the vertical development of clouds. A pending examination proposed to use the metrics introduced by Torri et al. (2017) and conduct a temporal analysis. If the metrics could prove statically significant in the past, perhaps information about cloud development in a future, warming climate could be realized. The latest, hourly European Reanalysis Dataset - ERA5 - offers the greatest temporal and spatial resolution proving to be the optimal dataset for the analysis. Unfortunately, the dataset provided on the supercomputer Cheyenne, or perhaps the dataset itself, is infested with a corrupt gribfile making it unusable. However, the ultimate goal of the research was to view the metrics on a monthly scale, and the monthly ERA5 dataset may prove to be a suitable alternative data source. As such, this report will be constructed around the framework laid out by Torri et al. (2017) (i.e., focus on the tropical Pacific, implementation of the convergence over evaporation metric, and focus given to the bulk surface latent heat flux equation).

2.1. Natural Fractionation of Stable Water Isotopes: Torri et al., 2017

The tropical ocean is well known to be a driving force in global climate variability, dominated by the Pacific Ocean and its teleconnections (Fairall et al., 1996). Unfortunately, convection and subsequent large-scale circulation in that region are still not fully understood (Torri et al., 2017). Due to the Walker Circulation, an east-west spatial variation in heating and vertical velocity structure exist in the region. Under normal conditions, the strong trade winds

result in warm (cold) surface water collecting in the west (east) and an unstable (stable) boundary layer (Zhang & McPhaden, 1994).

Torri et al. (2017) utilized the natural stratification of stable water isotopes in the atmosphere to further analyze the varying vertical profiles in the eastern and western tropical Pacific Ocean. Lighter water isotopes "float" to the upper portions of the atmosphere, leaving the lower pressure levels to be associated with the heavier counterparts. Consequently, clouds with a greater vertical extent tend to entrain a higher concentration of lighter water isotopes. In other words, taller clouds tend to have a more depleted ratio of water isotopes resulting in more depleted precipitation. The results of their investigation confirmed this relationship by finding precipitation in the tropical eastern pacific to be more enriched (higher amount of heavy water isotopes) than compared to the west. While their findings are intuitive with the Walker Circulation under normal conditions, the authors made a particular point to mention their findings differ from past reports, which found the opposite to be true.

2.2. Tropical Eastern Pacific

Torri et al. (2017) focused on vertical profiles within the tropical Pacific. However, the model used for the present report does not provide a high resolution mesh large enough to cover the entire tropical region (discussed further in subsection 3.2). As a first test of the different temporal ERAi datasets, this paper will focus on the tropical Eastern Pacific (EP).

Although the entire tropical ocean resides within the trade wind belt, the EP is dominated by the descending branch of the Walker Circulation and lower SST (refer to the previous subsection). The eastern side contains 90% of the cold water in the tropical ocean resulting in a low air-sea humidity difference and reduced LHF. While SST can reach above 300K during El Niño events, under normal conditions, the planetary boundary layer remains below the instability threshold, creating a strong, positive correlation between wind speed and LHF (Wu et al., 2007; Zhang & McPhaden, 1994).

2.3. Metrics

Given the focus of precipitation in the Torri et al. (2017) publication, the present work examines the impact of monthly and 6-hourly resolution datasets on SST directly, in addition to the latent heat bulk transfer equation (a function of SST), and the C/E index (a function of the latent heat flux). The cascading approach will help monitor the impact at various stages and determine if and when the different resolutions begin to matter.

2.3.1 Latent Heat Bulk Transfer

Surface heat fluxes are an important factor in model simulations focusing on climate variability (Wu et al., 2007). Using Reynolds averages and the related Monin-Obukhov similarity scaling parameters, the fluxes can be defined (Fairall et al., 1996). However, the

formulations are more commonly expressed in their standard bulk aerodynamic forms. Although the representation slightly varies amongst publications, the surface latent heat flux equation:

$$F_q = L_v \rho_a C_e U [q(T_s) - RH\, q(T)] \quad (1)$$

is parameterized by the latent heat of evaporation (L_v), air density (ρ_a), the turbulent transfers coefficient for latent heat (C_e), wind speed at 10m (U), in addition to the saturation water vapor mixing ratio as a function of sea surface temperature ($q(T_s)$) and air temperature at 10m ($q(T)$) multiplied by the relative humidity (RH) (Zhang & McPhaden, 1994). The latent heat flux has proven to have a much wider range of values (40 - 250 Wm^{-2}) relative to the sensible heat equivalent (Fairall et al., 2003). Up to ten percent of that uncertainty may be attributed to the transfer coefficients as the values stem from midlatitude field campaigns (Fairall et al., 1996).

Considering the first three terms in equation one are constant, wind speed and humidity are the dominant parameters. It is, therefore, pertinent to note the control sea surface temperature has on the flux of latent heat. Not only does SST have direct control on humidity, but Shindoa et al. (1998) suggest intraseasonal SST variations may significantly control the moisture content in the planetary boundary layer, indirectly influencing deep convection. At lower SST (<300K), the *latent heat flux increases with increasing SST*. As the surface warms, the saturation mixing ratio and subsequent evaporation increases. However, once above (approximately) 300K, the atmosphere becomes unstable, and the *latent heat flux decreases with increasing SST* (Figure 1). The change in trend is a consequence of convection. As the warm surface ocean destabilizes the planetary boundary layer, convection begins, and the surface experiences convergence of air. Due to mass continuity, at the center of the convergence, there is a local minimum wind speed and a subsequent dramatic decrease in the latent heat flux. In other words, under the 300K threshold, the humidity difference at the ocean-atmosphere interface is the dominant regulating parameter. Above 300K, wind speed controls the surface flux (Zhang & McPhaden, 1994).

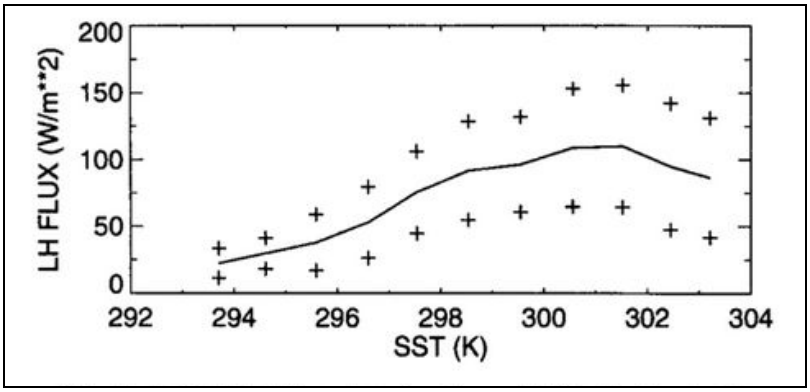

FIG 1. Latent heat flux as a function of SST. The curve represents the mean, and the "+" symbols represent the upper and lower bound of one standard deviation from the mean in each bin (Zhang & McPhaden, 1994).

2.3.2. Convergence/Evaporation (C/E)

Torri et al. (2017) propose a new metric termed convergence over evaporation. The authors included the index to account for the amount effect. Since their investigation involves isotopes, they note that rainfall rate, especially in the tropics, would preferentially remove the heavier stable water isotopes. Therefore, the greater the rainfall rates, the more depleted the cloud and subsequent precipitation become. However, instead of using precipitation rates directly from the model output, they created a similar metric to avoid errors often associated with the reanalysis datasets. The C/E index represents a ratio of water vapor that is vertically converged relative to the amount evaporated from the surface.

$$\frac{C}{E} = -\frac{1}{\rho_w \overline{q_v' \boldsymbol{v}'}} \int_{p_s}^{p_t} q_v \frac{\partial \omega}{\partial p} \frac{dp}{g} \tag{2}$$

The left-hand side of the integral denotes *evaporation* and is represented by the negative inverse of liquid water density (ρ_w) multiplied by a stand-in for the surface latent heat flux ($q'_v\mathbf{v}'$). However, this report will instead use the latent heat flux equation detailed above (Eq. 1). The remainder of the term is the integration from the surface to the tropopause of the partial change in omega ($\partial\omega/\partial p$) multiplied by the water vapor mixing ratio (q_v) and the inverse of gravity ($1/g$) (i.e., *convergence*). The authors also note that the term ignores horizontal advection of water vapor as it proved negligible (see Torri et al., 2017). A way to understand the metic would be to imagine evaporation is constant; in this case, the greater the layer of convergence, the more depleted the resulting precipitation (taller clouds, entrains lighter isotopes, more depleted rain).

3. Methods

3.1 Datasets

The 6-hourly and monthly ERAi datasets are accessible through NCARs high-performance computer, Cheyenne's online repository (ds627.0 and ds627.1, respectively). Both arrays have 0.703˚ x 0.702˚ spatial resolution from 180W to 180E and 89.46N to 89.46S and a temporal range from 1979-01-01 00:00 to 2019-09-10 12:00 (ECMWF, 2009; ECMWF 2012).

This report chose a three-month interval (DJF) from December 1997 to the end of February in the following year with two additional days at the end of November 1997 to allow for model spin-up. The specific range occurs during an Eastern Pacific El Niño event (Kiefer & Karamperidou, 2019), which had a period of unusually warm SST (2.2˚C) (NOAA, 2001). Under normal conditions, the tropical EP has low LHF variability, diminishing possible differences from using the different ERAi datasets (Wu et al., 2007). As noted in Fairall et al. (1996), an atmospheric model response is extremely sensitive to changes in anomalously warm SST. Therefore, an EP El Niño event would be the most challenging time for the two datasets to produce similar results making any discrepancies clear. If ERAi results match during the ENSO

event, it will provide confidence in using either dataset under normal conditions. Additionally, the focus on the winter season in the northern hemisphere avoids any impact MJO may have on the region (Maloney et al., 2002).

3.2 Model for Predictions Across Scales - Atmosphere (MPAS-A)

MPAS-A is used to simulate the impact of various temporal resolutions dataset on relevant variables. Developed by the National Center for Atmospheric Research (NCAR) and collaborators, MPAS-A is a non-hydrostatic model that allows for smoothly-varying transitions from a low spatial global resolution to high-resolution regional mesh (Fig. 2a) (Sharmarock et al., 2012). For the present report, a 60km to 15km mesh focuses on the tropical EP, spanning approximately 55 degrees of latitude and 110 degrees of longitude (Fig. 2b). Both domains have a vertical resolution of 50 levels.

WPS - WRF model Version 3 pre-processing system (Sharmarock et al., 2008) - converts the ERAi datasets into the required intermediate format. MPAS-A subsequently uses the files for the three-month simulation (DJF, 1997-1998). A 'mesoscale reference' physics scheme is applied, and the atmospheric model is forced with updated SSTs each time step to resolve a daily SST cycle.

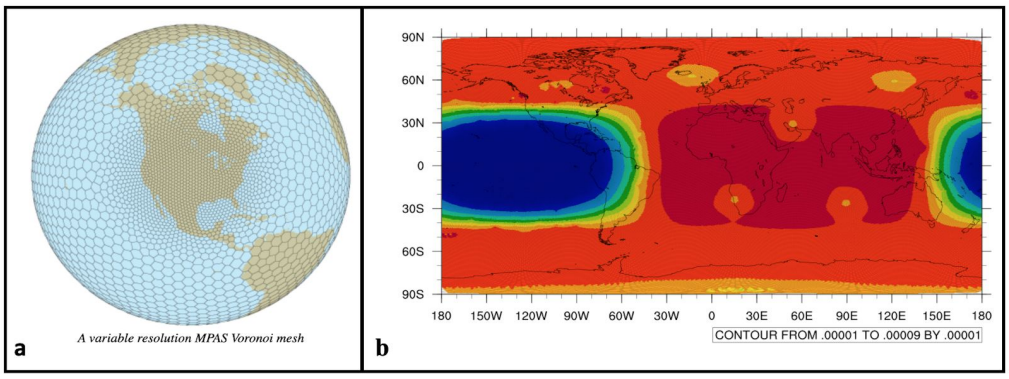

FIG. 2 (a) A visual representation of the smoothly-varying mesh focusing on North America **(b)** The 60km-15km mesh placement for the present report covering the tropical Eastern Pacific Ocean. The dark blue colors represent the high-resolution mesh (15km). The light blue, green, and yellow colors mark the transition from the high to low-resolution regions. The red colors mark the low-resolution (60km) mesh. The varying mesh's original position is marked by the "shadow" like shape covering the Atlantic and Indian Oceans.

3.3 Coding

Model output is then subjected to a series of interpolations and extrapolations (APPENDIX A) to produce the necessary variables comprising equations one and two. Additional manipulations are required to recreate the C/E index (APPENDIX B) before the results can be processed.

4. Results & Discussion

4.1 Sea Surface Temperatures (SST)

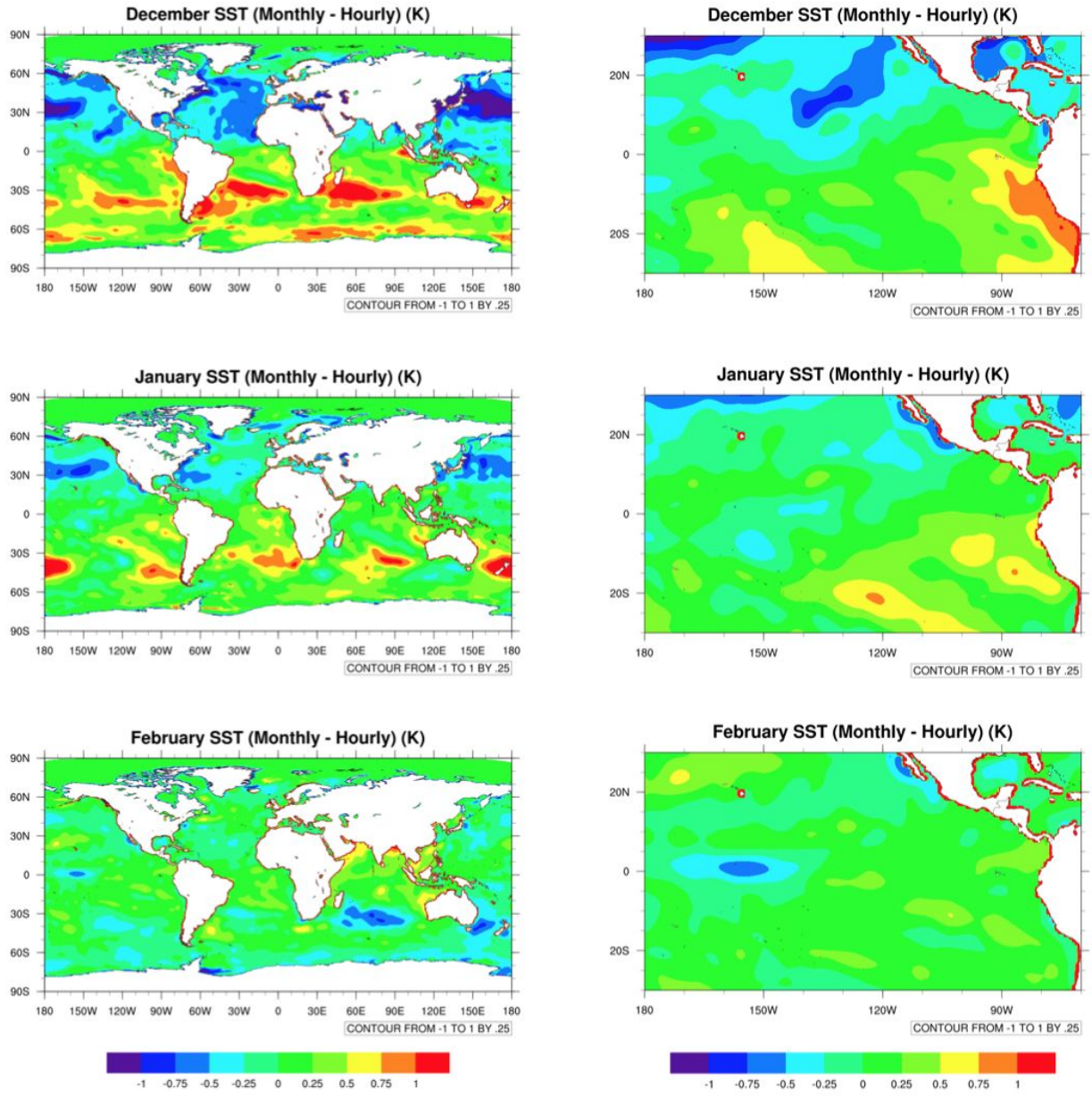

FIG 3. SST difference (monthly - 6-hourly) for December 1997, January, and February 1998. The left-hand side is from a global perspective, with most of the globe resolved down to 60km. The right-hand side is from a regional perspective of the tropical Eastern Pacific resolved down to 15km. The color bar ranges from ±1K.

The first output chosen for analysis is SST, as there is a well-understood positive correlation between SST, latent heat flux, and by extension, precipitation rates (Wu et al., 2007). The left-hand side of Figure 3 displays the global SST difference (monthly - 6-hourly) for December, January, and February. The right-hand side shows the regional perspective focusing on the highest resolution (15km) from the MPAS-A simulations, offering the highest accuracy. The yellow to red (blue) colors indicate regions where monthly (6-hourly) ERAi simulates a warmer SST. From a global scale, the northern and southern mid-latitudes display the most significant discrepancies reaching approximately ±1K, peaking in December and subsiding through February. A similar trend is present on the regional scale, but the area of interest is much less impacted by the temporal differences, especially when moving away from the coastlines. Although the SST difference is greater than anticipated, the model does reasonably well matching the anomalously warm SST conditions on both timescales and does not immediately disprove the use of either temporal resolution datasets when averaging on a monthly timescale.

4.2 Latent Heat Flux (LHF)

Figure 4 presents the latent heat flux equation (Eq. 1) formulated with the MPAS-A output. With the same configuration as Figure 3, the color bar now spans from ±50Wm^{-2}. Similar to SST, the differences reduce from December through February, but pockets of ±50Wm^{-2} are present in every month. A 'stripped' pattern is clear and appears to shift westward as the month progress. Present in both the global and regional scales, it is immediately apparent that there are immense differences between the monthly and 6-hourly ERAi datasets as any difference in latent heat flux greater than 10 Wm^{-2} is significant (Shindoa et al., 1998).

Although it is typical in the tropical Eastern Pacific for an anomalous SST to enhance surface evaporation and thus the latent heat flux (Wu et al., 2006; Zhang and McPhaden, 1994), this logic cannot explain the patterns as the SST for the monthly and 6-hourly timescale have a high level of agreement. A possible explanation may come from considering the 300K threshold (refer to subsection 2.3.1.). During the three-month analysis, nearly the entire tropical Eastern Pacific is dominated by SST at or above 300K (Appendix C). According to Zhang and McPhaden (1994), when above 300K, there is no dependence of the latent heat flux on SST, and the variation in the flux may be attributable to synoptic-scale fluctuation in weather or tropical instability waves. Perhaps the ERAi-6-hourly dataset is more sensitive to weather patterns than the monthly counterpart.

However, the most direct explanation for the pattern involves considering the variable connecting SST and the latent heat flux - surface specific humidity (APPENDIX D). Within the equatorial EP, the evaporation-SST correlation is dominated by the humidity gradient along with the ocean-atmosphere interface (Wu et al., 2006). The surface specific humidity plot has a similar oscillating positive and negative pattern covering the equatorial Pacific, suggesting that discrepancies begin with the parameterization of surface specific humidity as a function of SST (Eq. 2) and expands through the formulation of the LHF. Regardless of the reason for the different surface latent heat fluxes, it is a dominant control on the atmosphere-ocean system in

the tropical ocean (Zhang & McPhaden, 1994), undoubtedly influencing the vertical development of clouds within the region.

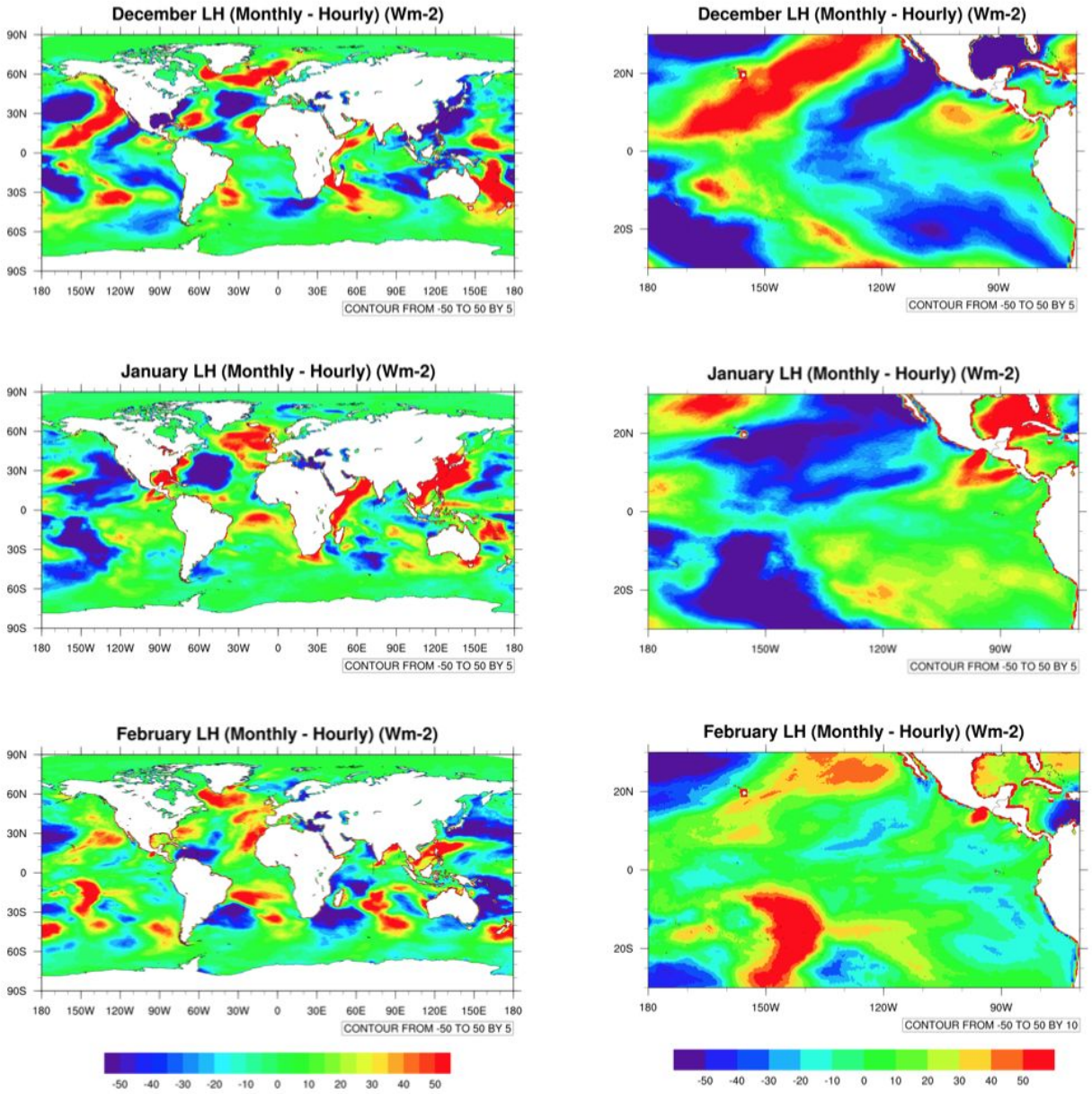

FIG 4. Latent heat flux difference (monthly - 6-hourly) for December 1997, January, and February 1998. The left-hand side is from a global perspective, with most of the globe resolved down to 60km. The right-hand side is from a regional perspective of the tropical Eastern Pacific resolved down to 15km. The color bar ranges from ± 50 Wm^{-2}.

4.3 Convergence/Evaporation (C/E)

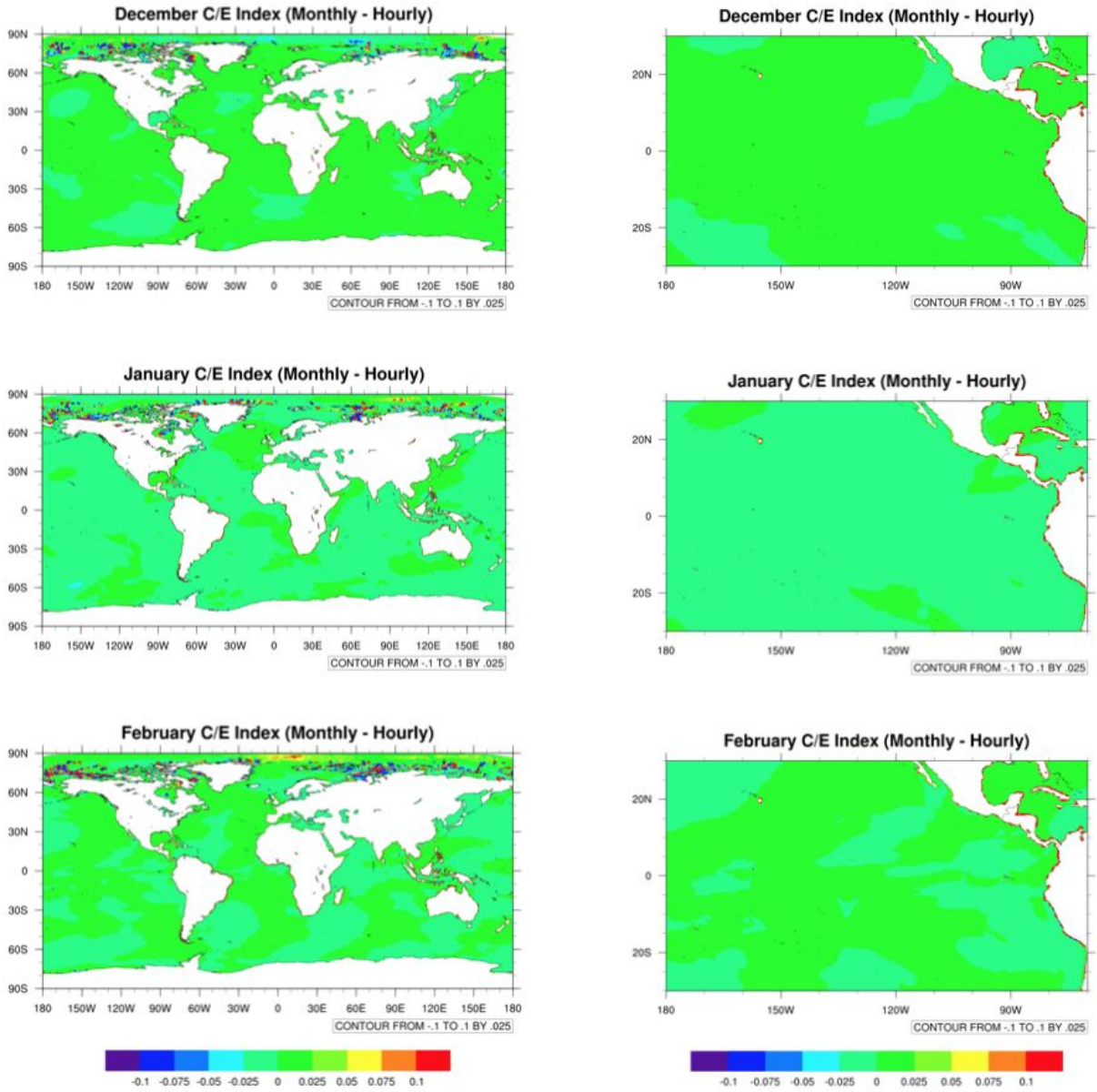

FIG 5. C/E (monthly - 6hourly) for December 1997, January, and February 1998. The left-hand side is from a global perspective, with most of the globe resolved down to 60km. The right-hand side is from a regional perspective of the tropical Eastern Pacific resolved down to 15km. The color bar ranges from ± 0.1.

Figure 5 presents the C/E index (Eq. 2) formulated with the MPAS-A output with the same configuration as the previous two figures. The color bar now spans from only ±0.1. Given the previous two results, this image is initially surprising. Unlike Figures 3 and 4, the C/E index shows remarkable agreement between the ERAi datasets. The figure shows either perfect agreement or negligible difference in the lower (60km) global resolution and the higher (15km) regional images.

Upon further investigation into the image, the magnitude of the evaporation and converge components of Equation 2 shows that the latter term's magnitude is serval orders larger than of the former. In other words, the formulation of the index gives more weight to the convergence terms. As described in subsection 2.3.2, the convergence term is the integration of the saturation mixing ratio, the partial change in omega over the partial change in pressure, and the inverse of gravity. Excluding gravity, as it is a constant value, the parameters of convergence can be quickly viewed through several plots (APPENDIX E). The high-resolution, regional view clearly shows a high agreement between ERAi datasets for both terms. The low variance of the convergence term allows for the large errors in LHF to be masked, resulting in the C/E plots above.

5. Conclusion

This report aimed to test if two datasets with different temporal resolutions are interchangeable when averaged over a month. The ERAi monthly and 6-hourly data is used to run a three month (DJF 1997 - 1998) simulation in the MPAS-A global climate model. The higher resolution (15km) varying mesh is focused in the tropical EP to analyze the SST, LHF, and C/E index, in addition to other associated or relevant variables. Strong (2.2˚C) El Niño conditions persisted during these months, increasing the SST in the relatively cold tropical EP region. The increase in surface temperature allows for large changes in the LHF to be observed, facilitating the comparison of temporal datasets.

The SST shows good agreement in the tropics but a larger difference in the mid and high latitudes reaching maximum values of ±1K. The variance approaches a peak in December and diminishes in the subsequent two months tested. Although the range of disagreement is small, if the ocean surface hovers about the 300K instability threshold, a 1K distinction could mean the difference between convection and stability, impacting future examination of the precipitation rates or vertical development of clouds.

LHF results show high variation between the ERAi monthly and 6-hourly datasets. Both the global low-resolution and regional high-resolution plots clearly show differences upwards of ±50 Wm^{-2}. Several speculative reasons are discussed for the high disagreements, but ultimately it is most likely the different ERAi resolution that is the primary source for the different flux rates. As values above 10 Wm^{-2} are significant (Shindoa et al., 1998), the LHF plots clearly suggest the variance between monthly and 6-hourly datasets is too significant to act as a substitute for one another in pending academic investigations.

Finally, the C/E index displayed high agreement across the globe with the datasets comparison. Although C/E is a function of the LHF, the higher-order magnitude of the convergence component of the term muted the high variance present in the LHF plots. The variables used to parameterize convergence are shown to have high agreeance, dominating the comparison of ERAi temporal resolution through the index. An argument can be made that the limited variance present in the C/E plots supports that either ERAi datasets are applicable for a future temporal test of Torri et al.'s (2017) metrics (outlined at the beginning of section 2). However, the extreme disagreement of the LHF and its fundamental relation to convections in the tropical EP is too strong of an argument to justify using any monthly ERA dataset in place of the 6-hourly equivalent.

6. References

Bretherton, Chris. “ATM S 547, Spring Quarter 2018.” Boundary-Layer Meteorology, atmos.washington.edu/~breth/classes/AS547/.

NOAA's Climate Prediction Center, (2001). Retrieved November 17, 2020, from https://origin.cpc.ncep.noaa.gov/products/analysis_monitoring/ensostuff/ONI_v5.php

European Centre for Medium-Range Weather Forecasts, 2009: ERA-Interim Project. Research Data Archive at the National Center for Atmospheric Research, Computational and Information Systems Laboratory, Boulder, CO. [Available online at https://doi.org/10.5065/D6CR5RD9.] Accessed 01 10 2020.

European Centre for Medium-Range Weather Forecasts, 2012: ERA-Interim Project, Monthly Means. Research Data Archive at the National Center for Atmospheric Research, Computational and Information Systems Laboratory, Boulder, CO. [Available online at https://doi.org/10.5065/D68050NT.] Accessed 01 10 2020.

Fairall, C. W., E. F. Bradley, D. P. Rogers, J. B. Edison, and G. S. Young (1996), Bulk parameterization of air-sea fluxes for Tropical Ocean-Global Atmosphere Coupled-Ocean Atmosphere Response Experiment, *J. Geophys. Res. Atmos., 101,* 3747-3764

Fairall, C. W., E. F. Bradley, J. E. Hare, A. A. Grachev, and J. B. Edison (2003), Bulk parameterization of air-sea fluxes: Update and Verification for the COARE Algorithm, *Am. Met. Soc.,* 571-591

Kiefer, J., & Karamperidou, C. (2019). High‐resolution modeling of ENSO‐induced precipitation in the tropical Andes: Implications for proxy interpretation. *Paleoceanography and Paleoclimatology*, *34*. https://doi.org/ 10.1029/2018PA003423

Maloney, E. D., and J. T. Kiehl, (2002): MJO-Related SST Variations over the Tropical Eastern Pacific during Northern Hemisphere Summer. *J. Climate*, *15*, 675–689, https://doi.org/10.1175/1520-0442(2002)015<0675:MRSVOT>2.0.CO;2.

Skamarock, W. C., J. B. Klemp, J. Dudhia, D. O., Gill, D. M. Barker, M. G. Duda et al. (2008). A description of the advanced research WRF Version 3. NCAR technical note NCAR/TN‐475+STR. https://doi.org/10.5065/D68S4MVH

Skamarock, W. C., J. B. Klemp, M. G. Duda, L. D. Fowler, S-H. Park, and T. D. Ringler (2012), A Multiscale Nonhydrostatic Atmospheric Model Using Centroidal Voronoi Tesselations and C-Grid Staggering, *Am. Met. Soc. 140,* 3090-3105.

Shindoa, T., H. H. Hendon, and J, Glick (1998), Intraseasonal Variability of Surface Fluxes and Sea Surface Temperature in the Tropical Western Pacific and Indian Ocean, *Am. Met. Soc., Vol 11,* 1685 - 1702

Torri, G., D. Ma, and Z. Kuang (2017), Stable water isotopes and large-scale vertical motions in the tropics, *J. Geophys. Res. Atmos.*, *122*, 3703–3717

Wu, R., B. P. Kirtman, and K. Pigeon (2006), Local Air-Sea Relationship in Observations and Model Simulations *Am. Met. Soc. 19,* 4914-4932

Wu, R., B. P. Kirtman, and K. Pegion (2007), Surface latent heat flux and its relationship with sea surface temperature in the National Centers for Environmental Prediction Climate

Forecast System simulations and retrospective forecasts, *Geophys. Res. Lett., 34*, L17712

Zhang, G. J., and M. J. McPhaden (1994) The relationship between Sea Surface Temperature and Latent heat Flux in the Equatorial Pacific. *Am. Met. Soc.,* 589-605

APPENDIX A

```
def hinterp(var):
      intf = np.zeros(var.shape)
      for i in range(len(var[0])): #535554 i (nCells)
      for j in range(len(var[0][0])): #55 j (nVertLevel)
            for k in range(len(var)): #3 k (Months)
                  try: intf[k,i,j] = 0.5*(var[k,i,j] + var[k,i,j+1])
                  except IndexError: pass
      return intf
#---------------------------------------------------------------------
def hextrapolater(ds):
      #---Define the function to extrapolate new vertical row
      def extrap_right(ds,height,row):
      from scipy import interpolate, arange
      #--- -1 to not include bottom row of 0's
      x = arange(len(ds[0][0])-1)
      y = ds[height,row,:-1]
      f = interpolate.interp1d(x, y, fill_value='extrapolate')
      return f(len(ds[0][0])-1)
      #
      #---Apply extrapolater to bottom of ds: output new row
      new_right = np.zeros((len(ds),len(ds[0]),1))
      for i in range(len(new_right[0])):
      for j in range(len(new_right[0][0])):
            for k in range(len(new_right)):
                  try: new_right[k,i,j] = extrap_right(ds,k,i)
                  except IndexError: pass
      #
      #---Combine new row to og ds (remove bottom row of 0s in og ds)
      new_ds = np.concatenate((ds[:,:,:-1],new_right),axis=2)
      #
      #---Flip the ds and repeate to create new top
      ds_rev = np.flip(new_ds, axis = 2)
      #
```

```
      #---Define the function to extrapolate new vertical row
      def extrap_left(ds,height,row):
      from scipy import interpolate, arange
      #--- -1 to not include bottom row of 0's
      x = arange(len(ds[0][0]))
      y = ds[height,row,:]
      f = interpolate.interp1d(x, y, fill_value='extrapolate')
      return f(len(ds[0][0]))
      #
      new_left = np.zeros((len(new_ds),len(new_ds[0]),1))
      for i in range(len(new_left[0])):
      for j in range(len(new_left[0][0])):
            for k in range(len(new_left)):
                  try: new_left[k,i,j] = extrap_left(ds_rev,k,i)
                  except IndexError: pass
      #
      #---Combine new top to og ds
      final_ds = np.concatenate((new_left,new_ds),axis=2)
      return final_ds
#-----------------------------------------------------------------------
def hinterp_exterp(ds):
      f1 = hinterp(ds)                  # u --> ui
      f2 = hextrapolater(f1)            # ui: LHS & RHS
      f3 = np.zeros(f2.shape)           # ui--> du
      for i in range(len(f3[0])):
      for j in range(len(f3[0][0])):
            for k in range(len(f3)):
                  try: f3[k,i,j] = f2[k,i,j+1] - f2[k,i,j]
                  except IndexError: pass
      f4 = f3[:,:,:-1]
      return f4
```

APPENDIX B

```
#---------LHS-------------------------------------------------------
rho_w = 997           # kg/m3
#
LHS = -1/(rho_w * lh) # ms3/kg2
LHS = np.reshape(LHS, (3,535554,1))
#---------RHS-------------------------------------------------------
g = 9.8               # m/s2
#
#---dp
dp = hinterp_exterp(p)
#
#---W
w = hinterp(wi)
w = w[:,:,:-1] #side get chopped via extrapolater
#
#---Omega
omega = -w * g * rho_w
domega = hinterp_exterp(omega)
#
#---domega/dp
domega_dp = domega/dp
#
def integrand(qv, domega_dp, g):
      return qv * domega_dp * 1/g
#
RHS = np.zeros((len(domega_dp),len(domega_dp[0]),1))
#
for k in range(len(domega_dp)):
      for j in range(len(domega_dp[0][0])):
      for i in range(len(domega_dp[0])):
            try: RHS[k,i,j] = quad(integrand,
                                   p[k,0,j], p[k,54,j],
                                   args=(qv[k,i,j], 1/g))[0]
            except IndexError: pass
#---------C_E-------------------------------------------------------
C_E = LHS * RHS
```

APPENDIX C

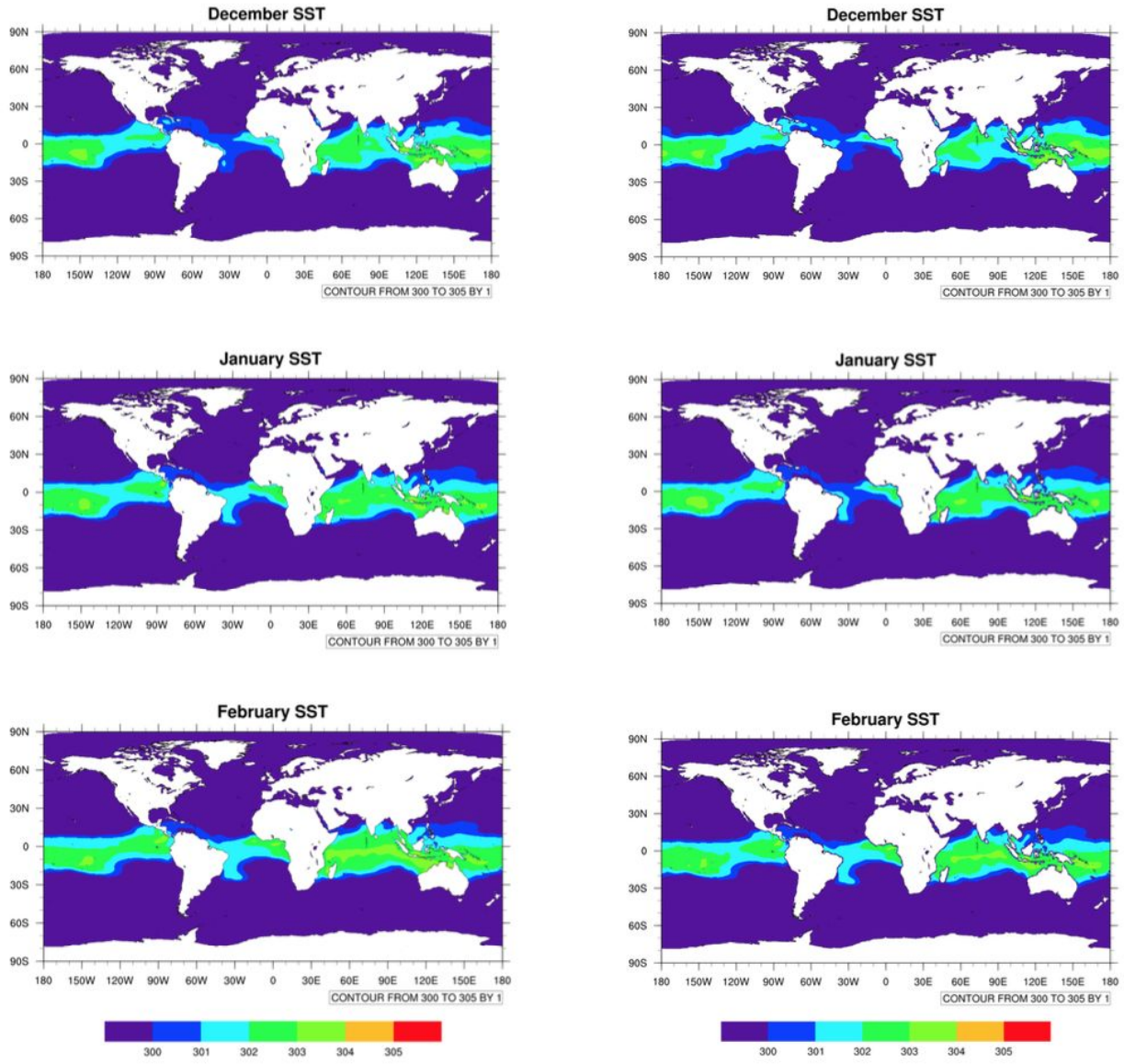

Global SST for December 1997, January, and February 1998. The color contrast highlights the regions over 300K with most of the globe resolved down to 60km. Regions in purple are below 300K, and regions colored blue and green are above 300K. The left-hand side is produced using the ERAi-monthly dataset. The right-hand side is produced using the ERAi-6-hourly dataset.

APPENDIX D

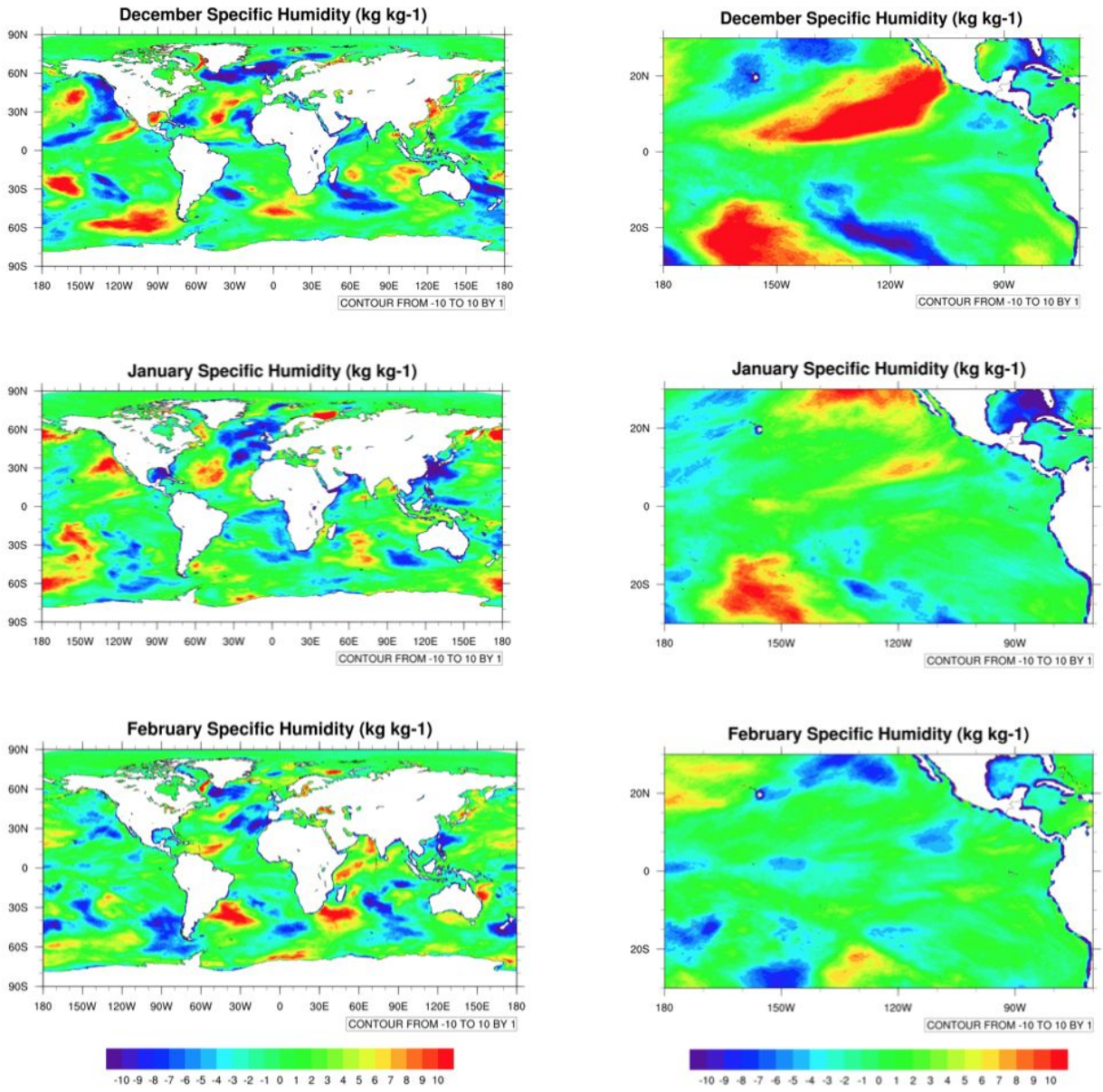

Specific humidity difference (monthly - 6-hourly) for December 1997, January, and February 1998. The left-hand side is from a global perspective, with most of the globe resolved down to 60km. The right-hand side is from a regional perspective of the tropical Eastern Pacific resolved down to 15km. The color bar ranges from ±10 kg kg^{-1}.

APPENDIX E

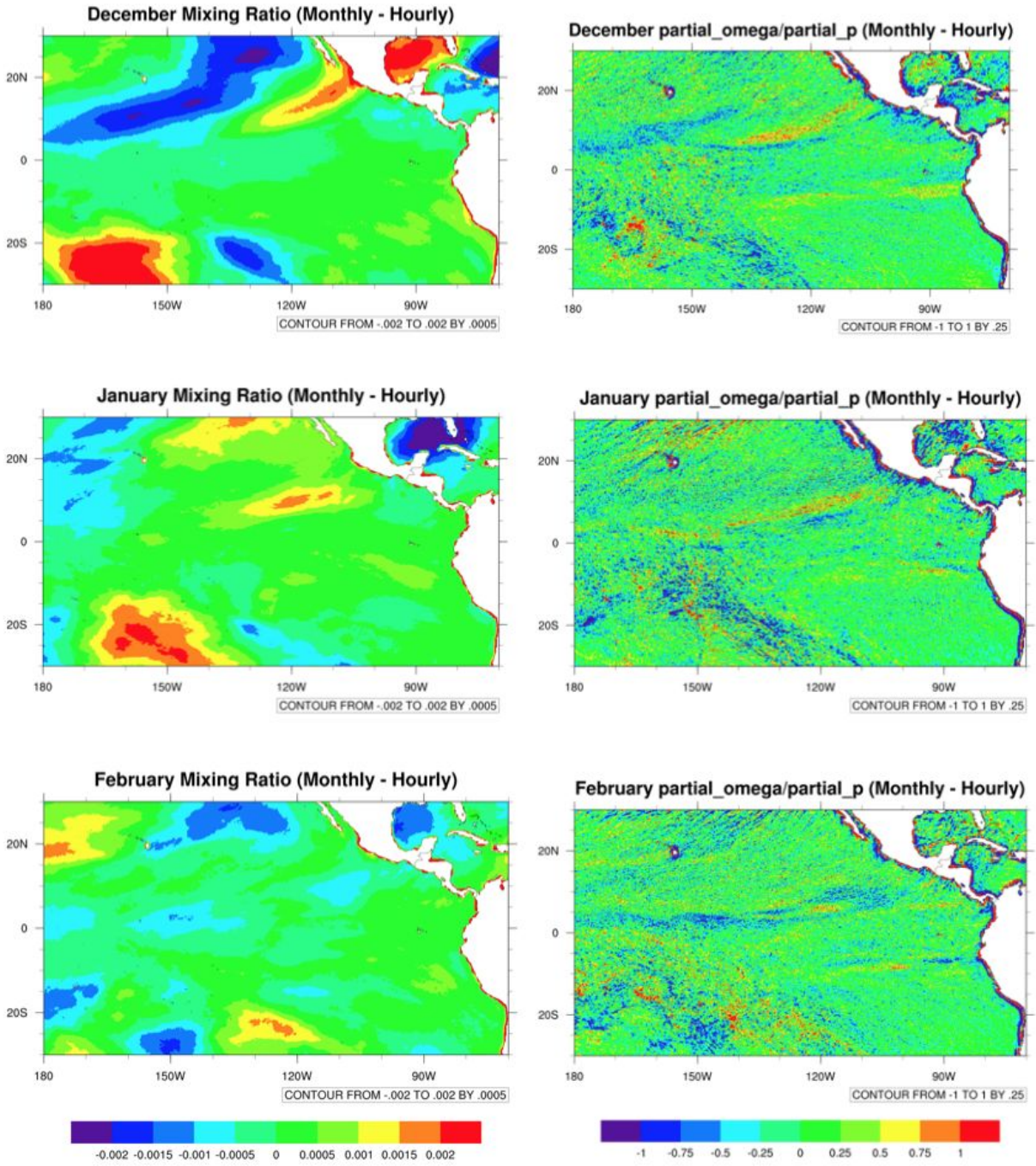

Regional plots in the tropical eastern Pacific with high-resolution (15km) mesh for December 1997, January, and February 1998. The left-hand side shows the saturation mixing ratio difference (monthly - 6-hourly) with a color bar ranging from ±0.002 kg kg^{-1}. The right-hand side shows the $\partial\omega/\partial p$ difference (monthly - 6-hourly) with a color bar ranging from ±01 ms^{-1}.